Electron beam melted beta-type Ti-24Nb-4Zr-8Sn porous structures with high strength-to-modulus ratio

Y.J. Liu[a,b], S.J. Li[b,*], W.T. Hou[b], S.G. Wang[b], Y.L. Hao[b], R. Yang[b], T.B. Sercombe[c], L.C. Zhang[a,**]

[a]*School of Engineering, Edith Cowan University, 270 Joondalup Drive, Joondalup, Perth, WA 6027, Australia*

[b]*Shenyang National Laboratory for Materials Science, Institute of Metal Research, Chinese Academy of Sciences, 72 Wenhua Road, Shenyang 110016, China*

[c]*School of Mechanical and Chemical Engineering, The University of Western Australia, 35 Stirling Highway, Perth, WA 6009, Australia*

Electron beam melting (EBM) has been used to manufacture β-type Ti-24Nb-4Zr-8Sn porous components with 70% porosity. EBM-produced components have advantageous structural features (i.e. smooth strut surfaces, fewer defects) and an (α+β)-type microstructure, similar to that formed after an aging treatment. EBM-produced components exhibit more than twice the strength-to-modulus ratio of Ti-6Al-4V porous components with same porosity. The processing-microstructure-property relationship and deformation behavior of EBM-produced components are discussed in detail. Such porous titanium components made using non-toxic elements and with high strength-to-modulus ratio and are therefore highly attractive for biomedical applications.

Keywords: Titanium alloys; Electron beam melting; Porous material; Mechanical properties; Microstructure

* Corresponding author. E-mail address: shjli@imr.ac.cn (S. J. Li)
** Corresponding author. E-mail addresses: lczhangimr@gmail.com, l.zhang@ecu.edu.au (L. C. Zhang).

Low-modulus, non-toxic β-type titanium alloys are regarded as the next generation implant materials for replacing dysfunctional bone tissues [1-8]. Ti-29Nb-13Ta-4.6Zr (TNTZ) [1], Ti-35Nb-7Zr-5Ta (TNZT) [3] and Ti-24Nb-4Zr-8Sn (Ti2448) [5] are examples of such novel alloys. However, they still possess a moduli (40-60GPa) much greater than bone (10-30GPa), which may cause stress shielding in the bone, leading to implant loosening or bone refracture. To avoid such issues, implant material should have a modulus closer to that of the bone it replaces. The modulus of a material can be reduced by introducing porosity. Further, the modulus of porous structure can be easily tailored and the bone cell growth can be more efficient compared to solid counterparts [8-13].

Recently, additive manufacturing (AM) technologies, such as electron beam melting (EBM) and selective laser melting (SLM), have received extensive attention due to the capability of producing complex porous components with attractive properties [8, 10-14]. Most studies on AM-produced porous titanium components are with (α+β)-type Ti-6Al-4V [8, 12] and α-type CP-Ti [10, 11] alloys. Along with the presence of toxic elements (i.e. Al, V), the presence of α' martensite in EBM-produced Ti-6Al-4V components causes brittleness and reduces the components' fatigue life [15]. However, very little work has been reported on processing, microstructure and properties of AM-produced β-type titanium porous components [13]. Because of its excellent properties [5, 6], β-type Ti2448 was applied by EBM technologies. SLM-/EBM-manufactured Ti2448 solid samples exhibit mechanical properties comparable to those by traditional methods [16, 17]. SLM/EBM-produced Ti2448 porous components have a lower modulus than solid components. From the point of view of biomechanical compatibility, an ideal implant material should have high permissible elastic strain, i.e., high strength-to-modulus ratio [18]. Therefore,

developing porous structures with high strength-to-modulus ratio is desirable for β-type titanium implants. This work reports the processing-microstructure-property relationship and mechanical behavior of EBM-produced Ti2448 porous components which exhibit a high strength-to-modulus ratio. The influence of electron beam scan speed on the properties of struts and the defects formed in the components have also been studied.

By repeating a single unit cell with size of 2×2×2mm^3, a porous structure model containing 7×7×14 unit cells, with a nominal 81% porosity (Fig. 1(a)) was constructed using Materialise Magics software. These components were then produced in an Arcam A1 EBM system, with build layer of 70μm, a voltage of 60kV and current of 3mA from Ti2448 powder, which had a particle size of 45-106μm. The build plate was preheated to 500°C to avoid smoking phenomenon during EBM process, which is much lower than 730°C used for Ti–6Al–4V [14]. After parameter optimization, EBM can produce near-fully dense components [19, 20]. Similar to SLM, the scan speed plays a critical role in producing high-quality components thereby affecting their properties [16, 21-23]. Increasing the scan speed reduces the input energy, affecting the microstructure and resultant properties of EBM-produced parts. As such, four sample groups (hereafter termed as Group A, B, C and D) were built at 150, 300, 600 and 900mm/s, respectively. The oxygen content of both the powder and EBM-processed components was measured to be 0.19 wt% using a TCH-600 O/N/H analyzer . The structure of the scaffolds was analyzed using a Zeiss Versa500 Micro-CT at an accelerating voltage of 160kV, current of 62.5μA, and voxel size of 13μm. 1600 projections were collected on a charge-coupled device detector using a 3s exposure time. In this work, the term pore is used for the deliberately created volumes within the unit cell while voids within the solid struts are termed

defects. Microstructural features were investigated by using an Olympus PMG-3 optical microscope (OM) and a Hitachi S-4700 Field Emission scanning electron microscope (SEM). Compressive tests were performed on three specimens for each Group using an Instron 5869 machine at strain rate of 0.5mm/min. Vickers mircohardness tests were conducted using Future Tech Fm-700 with a 100g load; 10 measurements on each sample were performed. Young's modulus was measured via compression testing [11, 12]. All mechanical property data shown are averaged results from multiple tests.

Fig. 1(a) also shows a side view of EBM-processed component. Fig. 1(b) shows XRD patterns for Ti2448 powder and EBM-fabricated components. Ti2448 powder contains a single β (bcc) phase. However, EBM-processed components consist of both α (hcp) and β phases, which is different from the single β phase found in EBM parts produced using a preheating of 250°C [17] or in SLM components [16]. As the build process took up to 10h, part had essentially been heat treated at ~500°C for 10h. This caused α phase formation during processing, similar to what occurs in Ti2448 that has been aged at 400-500°C [24]. Furthermore, the diffraction peaks of β phase slightly shift to a lower angle (Fig. 1(b)), due to dissolution of relatively more β-stabilizer Nb in the β phase resulting from the precipitation of α phase during EBM processing. The lattice parameter of β phase is ~3.310nm for EBM-processed components, which is larger than that for the powder (~3.296nm).

Figs. 1(c)-(f) illustrate the microstructure for Group A samples. The horizontal section of the struts consists of primarily aligned, long β grains (Fig. 1c). This phenomenon is caused by temperature gradient within build layers resulting from the electron beam scan tracks. It is apparent that α phase has formed only at β grain boundaries (Figs. 1(d) and (f)). In the vertical plane (Fig. 1(e)), elongated columnar grains formed in

build direction. Fusion lines (i.e. dark bands) generated during EBM process are also evident (Fig. 1(e)).

It has been reported that pore and strut size are important factors for bone cell regeneration in implants [25]. Surface area and the surface area to volume ratio, which are both closely related to the strut surface roughness, also play significant roles in bone cell regeneration. Micro-CT can provide a more accurate determination of the strut thickness and pore size compared to 2D images [26]. Fig. 2 shows reconstructed 3D visualization of the micro-CT data along with SEM micrographs of the outside surface of struts. Group A has smooth strut surfaces in all directions and also the best surface finish among all the Groups. For Group D, the balling effect is evident outside the surface (Fig. 2(d)) due to insufficient input energy [21].

The porosity of EBM-processed components was calculated by measuring the mass and volume of the structures and was found to be ~ 70% for all Groups, about 11 % lower than that of the CAD model used. Fig. 3(a) shows distributions of pore and strut sizes and their average values for EBM-produced scaffolds. The strut size for Groups A-D was 439±40, 438±43, 443±56 and 401±63μm, respectively, resulting in smaller pores and therefore less porosity in comparison to the computer model. Except for Group D, the average strut size was almost constant. Fig. 3(b) shows shape and distribution of the defects (voids) for all Groups. Defects are spherical and appear to be randomly distributed. Both the size and count vary significantly with electron beam scan speed. For the slower scan speeds (Groups A and B) there are less defects and these tend to be smaller in size in comparison to high speeds (Groups C and D). Such phenomena are attributed to low scan speed causing poor-quality melt traces due to Marangoni flow [27]. Murr et al [28] indicated that small defects can result from argon gas entrapped in starting powder whilst large defects are formed during the

EBM process at insufficient input energy. Another possibility of forming defects is vaporization of metal, which is known to occur during laser processing [13, 29].

As seen in Table 1, Ti2448 has lower microhardness than Ti-6Al-4V; Ti2448 with α+β phases has higher microhardness than those with single β phase. Group D samples have slightly lower strength than Group A-C parts (Fig. 4(b)). In addition, Group A parts exhibit higher compressive strength (37 MPa) than Ti-6Al-4V (31 MPa [14]) at same porosity level and produced using the same unit cell. Groups A-C essentially shows identical mechanical performance in terms of the first strut failure strength and plasticity; the first strut failures occur at a stress of 33-37 MPa. However, Group D has lower mechanical properties; the strut first fails at 27 MPa. The mechanical performance is closely associated with the average strut size. Although containing plenty of defects, Group C parts still exhibit good mechanical properties. Therefore, strut size rather than amount of defects appears to be the main factor influencing mechanical performance of EBM-processed scaffolds.

Scan speed also significantly affects Young's modulus. The values of Young's modulus for Groups A-D are 0.93±0.06, 0.85±0.11, 0.83±0.13 and 0.7±0.14 GPa, respectively. For the same Young's modulus of 0.86 GPa, Ti2448 porous components have ~2 times the compressive strength of Ti-6Al-4V with same unit cell (20 MPa [14]). As seen from Table 1, EBM-processed Ti2448 porous components have at least twice the strength-to-modulus ratio of Ti-6Al-4V porous components with same porosity of 70%.

Fracture surfaces of struts are shown on the right hand of Fig 2. Quasi-cleavage facets with ductile dimples are observed for all components. Fracture surfaces contain several large pores and dimples in Group B (Fig. 2(b)) and C (Fig. 2(c)). For Group D (the fastest scan speed), unmelted particles are evident in the struts and its fracture

surface shows smooth zones related to intergranular fracture (Fig. 2(d)). In addition, Group D parts contain a higher fraction of smooth regions related to brittle fracture in fracture surfaces than A-C Groups.

In summary, β-type Ti2448 porous structures with 70% porosity have been fabricated using EBM. Lower electron beam scan speed leads to more input energy thereby producing stronger struts with fewer defects. This resulted in better mechanical properties and at least twice the strength-to-modulus ratio of Ti-6Al-4V porous components with same porosity. The excellent properties are attributed to precipitation of α phase at β grain boundaries due to high-temperature preheating in EBM process.Such non-toxic Ti2448 porous components with very high strength-to-modulus ratio are highly attractive for biomedical applications.

This work was supported partially by National Natural Science Foundation of China (51271182, 51271180), National Basic Research Program of China (2012CB619103, 2012CB933901), 863 Project (2015AA033702) and Australian Research Council Discovery Project (DP110101653).

[1] M. Niinomi, Biomater., 24 (2003) 2673-2683.
[2] M. Geetha, A.K. Singh, R. Asokamani, A.K. Gogia, Prog. Mater. Sci., 54 (2009) 397-425.
[3] J.I. Qazi, B. Marquardt, L.F. Allard, H.J. Rack, Mater. Sci. Eng. C, 25 (2005) 389-397.
[4] S.E. Haghighi, H.B. Lu, G.Y. Jian, G.H. Cao, D. Habibi, L.C. Zhang, Mater. Des., 76 (2015) 47-54.
[5] Y.L. Hao, S.J. Li, S.Y. Sun, C.Y. Zheng, Q.M. Hu, R. Yang, Appl. Phys. Lett., 87 (2005) 1906.
[6] Y.L. Hao, S.J. Li, S.Y. Sun, C.Y. Zheng, R. Yang, Acta biomater., 3 (2007) 277-286.
[7] S.J. Li, T.C. Cui, Y.L. Hao, R. Yang, Acta biomater., 4 (2008) 305-317.
[8] X.Y. Cheng, S.J. Li, L.E. Murr, Z.B. Zhang, Y.L. Hao, R. Yang, F. Medina, R.B.

Wicker, J. Mech. Behav. Biomed. Mater., 16 (2012) 153-162.
[9] G. Ryan, A. Pandit, D.P. Apatsidis, Biomater., 27 (2006) 2651-2670.
[10] H. Attar, M. Bönisch, M. Calin, L.C. Zhang, K. Zhuravleva, A. Funk, S. Scudino, C. Yang, J. Eckert, J. Mater. Res., 29 (2014) 1941-1950.
[11] H. Attar, L. Löber, A. Funk, M. Calin, L.C. Zhang, K.G. Prashanth, S. Scudino, Y.S. Zhang, J. Eckert, Mater. Sci. Eng. A, 625 (2015) 350-356.
[12] V.J. Challis, X. Xu, L.C. Zhang, A.P. Roberts, J.F. Grotowski, T.B. Sercombe, Mater. Des., 63 (2014) 783-788.
[13] Y.J. Liu, X.P. Li, L.C. Zhang, T.B. Sercombe, Mater. Sci. Eng. A, 642 (2015) 268-278.
[14] S.J. Li, Q.S. Xu, Z. Wang, W.T. Hou, Y.L. Hao, R. Yang, L.E. Murr, Acta biomater., 10 (2014) 4537-4547.
[15] S.J. Li, L.E. Murr, X.Y. Cheng, Z.B. Zhang, Y.L. Hao, R. Yang, F. Medina, R.B. Wicker, Acta Mater., 60 (2012) 781–792.
[16] L.C. Zhang, D. Klemm, J. Eckert, Y.L. Hao, T.B. Sercombe, Scripta Mater., 65 (2011) 21-24.
[17] J. Hernandez, S.J. Li, E. Martinez, L.E. Murr, X.M. Pan, K.N. Amato, X.Y. Cheng, F. Yang, C.A. Terrazas, S.M. Gaytan, J. Mater. Sci. Tech., 29 (2013) 1011-1017.
[18] S.J. Li, Y.L. Hao, R. Yang, Y.Y. Cui, M. Niimomi, Mater. Trans., 43 (2002) 2964-2969.
[19] L.E. Murr, S.M. Gaytan, F. Medina, E. Martinez, J.L. Martinez, D.H. Hernandez, B.I. Machado, D.A. Ramirez, R.B. Wicker, Mater. Sci. Eng. A, 527 (2010) 1861-1868.
[20] S. Biamino, A. Penna, U. Ackelid, S. Sabbadini, O. Tassa, P. Fino, M. Pavese, P. Gennaro, C. Badini, Intermetallics, 19 (2011) 776-781.
[21] H. Attar, M. Calin, L.C. Zhang, S. Scudino, J. Eckert, Mater. Sci. Eng. A, 593 (2014) 170-177.
[22] H. Attar, K.G. Prashanth, A.K. Chaubey, M. Calin, L.C. Zhang, S. Scudino, J. Eckert, Mater. Lett., 142 (2015) 38-41.
[23] H. Attar, M. Bönisch, M. Calin, L.C. Zhang, S. Scudino, J. Eckert, Acta Mater., 76 (2014) 13-22.
[24] T.C. Cui, L.S. J., Y.L. Hao, R. Yang, Chin. J. Mater. Res., 22 (2008) 225-229.
[25] K.F. Leong, C.M. Cheah, C.K. Chua, Biomater., 24 (2003) 2363-2378.
[26] S. Van Bael, Y.C. Chai, S. Truscello, M. Moesen, G. Kerckhofs, H. Van Oosterwyck, J.P. Kruth, J. Schrooten, Acta biomater., 8 (2012) 2824-2834.
[27] I. Yadroitsev, P. Bertrand, I. Smurov, Appl. Surf. Sci., 253 (2007) 8064-8069.
[28] S.M. Gaytan, L.E. Murr, F. Medina, E. Martinez, M.I. Lopez, R.B. Wicker, Mater. Sci. Tech., 24 (2009) 180-190.
[29] K.A. Mumtaz, P. Erasenthiran, N. Hopkinson, J. Mater. Proc. Tech., 195 (2008) 77-87.

Table 1 Compressive mechanical properties, Vickers hardness (HV) and phase constituents of EBM- and SLM-manufactured titanium materials. Young's modulus E, ultimate strength σ_{max}, and strength-to-modulus ratio σ_{max}/E.

Material	Method	Phase constituent	HV	E (GPa)	σ_{max} (MPa)	σ_{max}/E ($\times 10^{-3}$)	Ref
Ti2448 (solid)	EBM	β	250	…	…	…	[17]
Ti2448 (solid)	SLM	β	228±6	53±1[a]	665±18[a]	12.5	[16]
Ti2448 (70% porosity)	EBM	α+ β	280±5	0.7±0.1	35±2[b]	~50	This work
Ti6Al4V (70% porosity)	EBM	α+ β	331±14	~1	~20[b]	~20	[14]
CP-Ti (37 porosity)	SLM	α+α′	261±13 [10]	13±3	235±52	18.1	[11]
Ti-8.35vol.% TiB (37 porosity)	SLM	α+ β	402±7 [23]	25±2	256±4	10.2	[11]

[a]in tension; [a]first strut failure strength

Figure Captions

Fig. 1 (a) Porous structure model used and side view of EBM-processed component, (b) XRD profiles of the starting powder and EBM-processed components, (c) and (e) OM, and (d) and (f) SEM images of Group A. (c)-(d) are at horizontal plane and (e)-(f) are vertical views.

Fig. 2 Micro-CT (left) and SEM surface morphology (middle) of single unit cell and SEM fracture morphology (right) for Groups: (a) A, (b) B, (c) C, and (d) D.

Fig. 3 (a) Distribution and average value of strut and pore size, and (b) defects distribution analyed from micro-CT. Defects inside struts have been coloured black.

Fig. 4 The stress-strain curves for EBM-processed components.

Figures + caption: 11x20+10x20+12x20+6.5x20+109=899

Table + caption: 3x40+27=147

Texts: 2410

Equivalent texts in total: 2410+899+147=3456

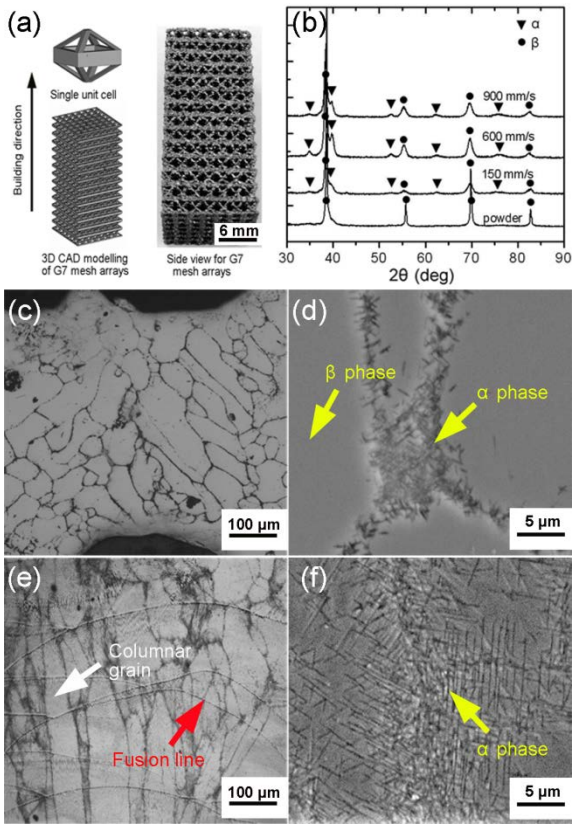

Fig 1. Y.J. Liu *et al*

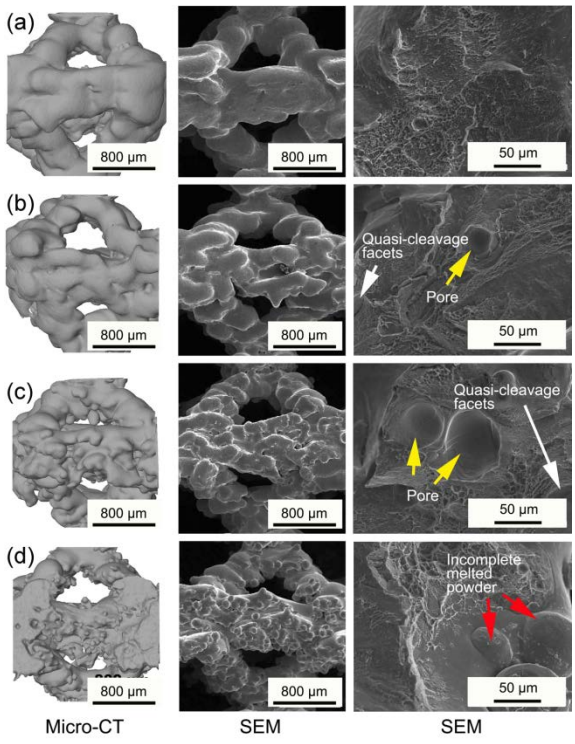

Fig 2. Y.J. Liu *et al*

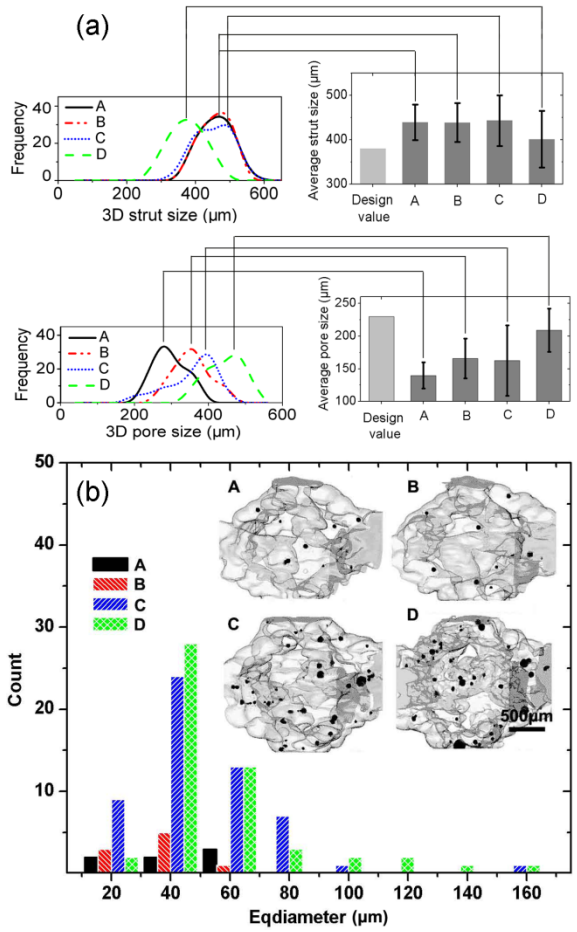

Fig 3. Y.J. Liu *et al*

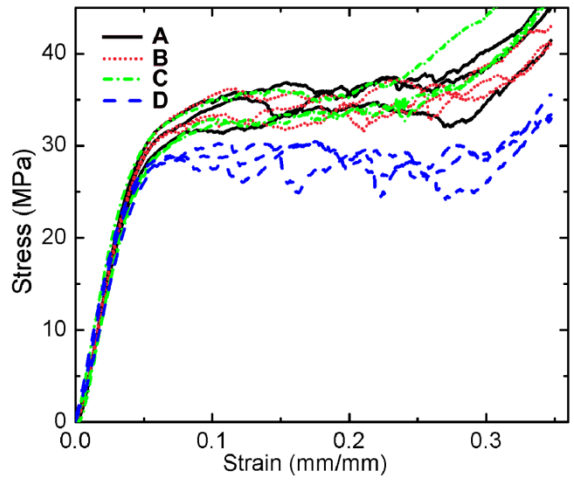

Fig 4. Y.J. Liu *et al*